Model-Based Dynamic Control of Two Degrees-Of-Freedom Modulation for Dual Active Half-Bridge Converter

Gun-Su Kim[1], Su-Bin Kang[1], Hyeon-Sik Kim[1], Jehyuk Won[2]
[1] Department of Electrical Engineering, Gachon University, Republic of Korea
[2] Department of Smart City and Energy, Gachon University, Republic of Korea

***Abstract*—This paper proposes a model-based dynamic control for dual active half-bridge converters to satisfy both a loss-minimizing operation and a high-dynamic response. First, the loss-minimizing operation is analyzed based on a two degrees-of-freedom (DOF) modulation scheme, where two variables, a phase shift and a duty ratio, are determined to minimize a transformer rms current. The 2-DOF modulation could be changed to the 1-DOF modulation according to operating conditions, where a smooth transition between the modulation schemes is required. Moreover, the output voltage control should be designed to provide fast dynamic performance under source and load variations. Therefore, the voltage controller is unified with the modulation schemes where a model-based control is adopted to lessen the burden of an error compensation part. A model-based calculation part improves the dynamics of the 2-DOF modulation with a load current feedforward. Lastly, the effectiveness of the proposed method is verified by the simulation and experimental results.**

***Index Terms*— Dual active half-bridge converter (DAHB), minimum rms current, modulation scheme, model-based control.**

I. Introduction

A dual active bridge (DAB) dc-dc converter has been widely adopted in many applications owing to the advantages such as zero-voltage switching, bi-directional power flow capability and convenience of cascading and paralleling [1]-[3]. Compared to the dual active bridge (DAB) converter with a full-bridge structure, the DAHB converter with a half-bridge structure can reduce the number of a power MOSFET and its driving circuit by applying split dc capacitors on both sides. Thus, it is preferred in a low-power system (below 750 W) because the cost, volume, and weight of the converter can be minimized compared with the DAB converter [4]-[6].

In the DAHB converter, the phase could be shifted from −90° to +90° for changing the power transfer between a primary and a secondary side. For the maximum power transfer, the duty ratio is fixed to 0.5 and the phase shift is controlled to regulate the output voltage. It has been called the single-phase shift (SPS), which is equivalent to a single degree-of-freedom (1-DOF) modulation. Moreover, the duty ratio could be varied to introduce different average voltages on the split dc capacitors in the light-load condition. Therefore, the converter efficiency can be improved with suppressed high-circulating current. It has been called the asymmetric duty control, which is referred as a two degrees-of-freedom (2-DOF) modulation.

Several 2-DOF modulation schemes have been reported to improve the system efficiency [3], [6]. They improve the system efficiency by minimizing rms current or extending zero voltage switching (ZVS) range. However, the 2-DOF modulations are mostly implemented by two PI controllers with different bandwidth, where the duty ratio is controlled by an inner slow control loop after the phase shift is adjusted [6], [7]. This control scheme is easy to implement and suppresses the interference between the control loops with different dynamics. However, the transient responses such as source and load changes would be deteriorated due to the slow control dynamics. Moreover, the transitions between the 1-DOF and 2-DOF modulation schemes were not considered. The dynamics of the DAHB converter should be analyzed to not only increase the control bandwidth but also provide the smooth transition.

Generally, the proportional-integral (PI) controller is adopted to regulate the output voltage where a load current feedforward (LCFF) could be added to improve the transient response. However, this conventional method is difficult to achieve linear dynamic characteristics due to a nonlinear relationship between the phase shift and the power transfer. The look-up table (LUT) solution could be applied to overcome these constraints. However, the LUT methods require a large memory usage and an accurate interpolation algorithm to minimize an approximation error. Recently, a model-based control has been applied in case of the DAB converter to improve the control dynamics. It has been modeled based on the power transfer equation where the effects of input voltage, output voltage, and load current are fully considered [8]-[10]. Likewise, the model-based voltage controller with the feedforward loop could be designed for the DAHB converter. This improves the dynamic response under the transient conditions, which means the robustness against input voltage and load current disturbances.

In this paper, the 2-DOF modulation scheme is analyzed to minimize a transformer rms current where the power transfer equation is derived as the function of the phase shift and the duty ratio. This modulation scheme is unified with the model-based voltage controller, which consists of an error compensation part and a model-based calculation part. The calculation process is inserted in the output of the

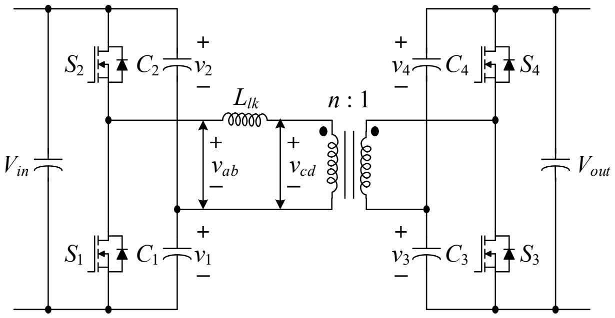

Fig. 1. Topology of the dual active half-bridge (DAHB) converter.

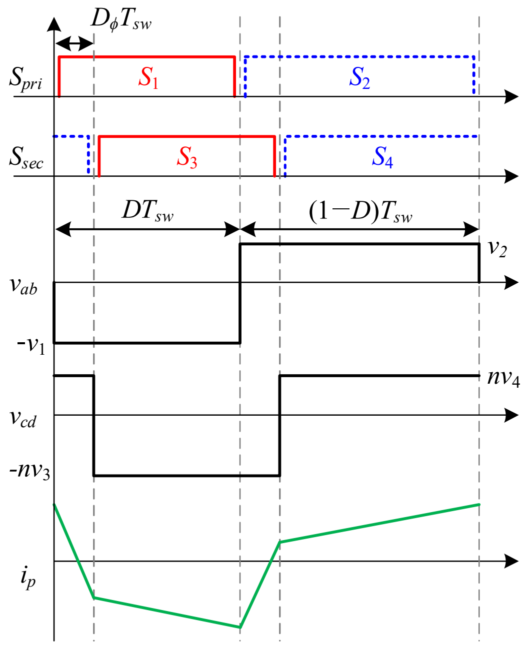

Fig. 2. Typical operating waveforms of 2-DOF modulation.

PI controller with LCFF to derive 2-DOF modulation references, i.e., the phase shift reference and the duty ratio reference. The performance of the proposed controller is verified by simulation and experimental results. The dynamic response of the proposed method could be improved compared with that of the conventional method under not only the load changes but also the input voltage and the output voltage reference variations.

II. Operating Principle of DAHB Converter

Fig. 1 shows a circuit schematic of the DAHB converter. The input voltage dc port, V_{in}, is interfaced with the output voltage dc port, V_{out}, where S_1, S_2 is primary-side half-bridges and S_3, S_4 is secondary-side half-bridges. The primary- and secondary-side transformer voltage represent v_{ab} and v_{cd}, respectively, which are referred to the input port. Moreover, L_{lk} denotes a primary-referred leakage inductance of the transformer and n represents a turn ratio.

Fig. 2 shows the typical operating waveforms of gate signals, transformer voltages, and currents where the 2-DOF modulation is applied. The duty ratio for the low-side switches is defined as D, and the phase shift is defined as $D_\phi T_{sw}$, where T_{sw} is the switching time, i.e., $1/f_{sw}$. In this case, the split dc capacitor voltages from v_1 to v_4 is determined by the flux-second balance of a leakage inductance of the transformer, L_{lk}. The primary-side current of the transformer, i_p, is piecewise linear according to the switching patterns.

For the 2-DOF modulation control, the transferred power, P, can be calculated as (1), where $P > 0$ means that the power is transferred from input port to output port.

$$P(D,D_\phi) = CD_\phi\left[2D(1-D)-\left|D_\phi\right|\right], \tag{1}$$

where $C = \dfrac{nV_{in}V_{out}}{2L_{lk}f_{sw}}$.

Otherwise, $P < 0$ represents the power is transferred from output port to input port, i.e., regenerative operation. In addition, the rms current of the primary-side, $I_{p(rms)}$, is defined as (2), which can be derived as the function of D and D_ϕ from the current waveform in Fig. 2 [6].

$$I^2_{p(rms)}(D,D_\phi) = k[aD^2(1-D)^2 + bD_\phi^2(3D(1-D)-\left|D_\phi\right|)], \tag{2}$$

where $M = (nV_{out})/V_{in}$ means an effective voltage conversion ratio; $k = V_{in}^2/(12L_{lk}^2 f_{sw}^2)$, $a = (1-M)^2$, and $b = 4M$.

III. Minimum RMS Current Operation

The 2-DOF modulation could be applied to minimize the transformer rms current, which suppresses the high-circulating current in the circuit, i.e., conduction loss reduction of the switches and the transformer. Thus, the minimum current operation of the DAHB converter is stated as the following optimization problem in (3). It can derive the phase shift reference, $D_{\phi,ref}$, and the duty ratio reference, D_{ref}.

$$\begin{aligned} &\text{minimize} && I^2_{p(rms)}(D_{ref}, D_{\phi,ref}), \\ &\text{subject to} && G_V(D_{ref}, D_{\phi,ref}) = G_{V,ref}. \end{aligned} \tag{3}$$

The virtual conductance, G_V, is derived from the power equation in (1) to simplify the calculation process as follows.

$$G_V(D,D_\phi) = \frac{P(D,D_\phi)}{C} = D_\phi\left[2D(1-D)-\left|D_\phi\right|\right] \tag{4}$$

Likewise, the virtual conductance reference, $G_{V,ref}$, is defined as the function of the output current reference over the input voltage, I_{ref}/V_{in}, as follows, where the effects of output voltage, V_{out}, is removed.

$$G_{V,ref} = \frac{P_{ref}}{C} = \frac{2L_{lk}f_{sw}}{nV_{in}}\frac{P_{ref}}{V_{out}} = \frac{2L_{lk}f_{sw}}{n}\frac{I_{ref}}{V_{in}} \tag{5}$$

Equation (3) can be solved by the Lagrange multiplier method, where a Lagrangian function is defined as (6), and μ is a Lagrange multiplier, respectively.

$$\begin{aligned} \mathcal{L}(D_{ref}, D_{\phi,ref}, \mu) = {} & I^2_{p(rms)}(D_{ref}, D_{\phi,ref}) \\ & + \mu[G_{V,ref} - G_V(D_{ref}, D_{\phi,ref})]. \end{aligned} \tag{6}$$

In this case, the maximum duty ratio is 0.5 and the phase shift, D_ϕ, is limited within [-0.25 to 0.25] to minimize the rms current under the same power.
It is formulated as a pair of equations with two unknowns, D_{ref} and $D_{\phi,ref}$ as follows.

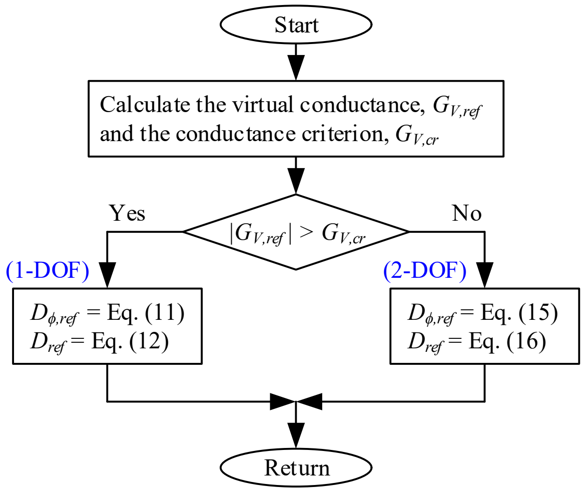

Fig. 3. Flowchart for the 2-DOF modulation calculation.

$$G_{V,ref} = D_{\phi,ref}\left[2D_{ref}(1-D_{ref}) - \left|D_{\phi,ref}\right|\right]. \tag{7}$$

$$D_{ref}(1-D_{ref}) = \frac{1}{2\alpha} D_{\phi,ref}{}^2 + \left|D_{\phi,ref}\right|, \text{ where } \alpha = \frac{a}{3b}. \tag{8}$$

Equation (7) indicates the virtual conductance equation derived from the constraint condition in (3). Equation (8) represents the minimum current operation where the current output matches the current reference.

The solutions are divided into the case of 1-DOF modulation ($D_{\phi,ref}$) and the case of 2-DOF modulation ($D_{\phi,ref}$, D_{ref}) according to the absolute magnitude of the current reference, $|I_{ref}|$. The modulation scheme can be determined by the comparison between the virtual conductance reference, $G_{V,ref}$, and the conductance criterion, $G_{V,cr}$. $G_{V,cr}$ represents the modulation criterion between the 1-DOF and 2-DOF control where D_{ref} is set to 0.5 for both cases. It can be solved by substituting D_{ref} with 0.5 for (7) and (8) in the condition of $D_{\phi,ref} > 0$ [6]. As a result, $G_{V,cr}$ is derived as follows.

$$G_{V,cr} = D_{\phi,cr}(0.5 - D_{\phi,cr}). \tag{9}$$

$$D_{\phi,cr} = -\alpha + \sqrt{\alpha^2 + \frac{1}{2}\alpha}. \tag{10}$$

When $|G_{V,ref}|$ exceeds $G_{V,cr}$, D_{ref} is fixed with 0.5 to maximize the transfer power and $D_{\phi,ref}$ is adjusted to satisfy the constraint in (7), i.e., the region of 1-DOF control. For the 1-DOF control, $D_{\phi,ref}$ can be calculated using the quadratic formula as follows.

$$D_{\phi,ref} = sign(G_{V,ref})\frac{1-\sqrt{1-16\left|G_{V,ref}\right|}}{4}. \tag{11}$$

$$D_{ref} = 0.5. \tag{12}$$

When $|G_{V,ref}|$ is below $G_{V,cr}$, the 2-DOF control could be implemented by solving the simultaneous equations in (7) and (8) as follows.

$$D_{\phi,ref}{}^3 + \alpha(D_{\phi,ref}\left|D_{\phi,ref}\right| - G_{V,ref}) = 0. \tag{13}$$

$$D_{ref}{}^2 - D_{ref} + \frac{1}{2\alpha}D_{\phi,ref}{}^2 + \left|D_{\phi,ref}\right| = 0. \tag{14}$$

Equation (13) is a cubic equation of $D_{\phi,ref}$ by substituting (7) with (8), where D_{ref} is removed. Equation (14) is deduced from (8).

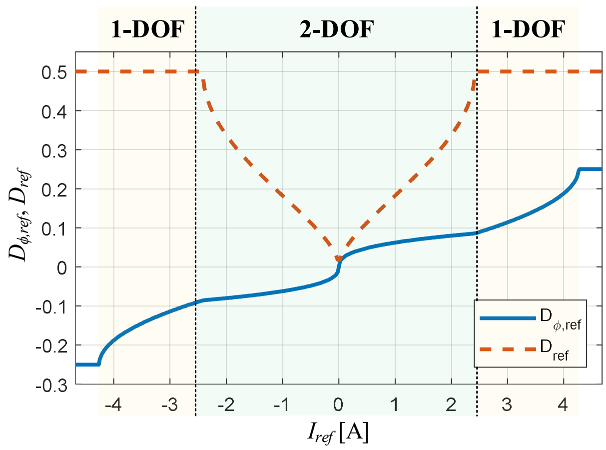

Fig. 4. Trajectories of phase-shift reference and duty ratio reference when $M = 0.6$.

TABLE I. SYSTEM PARAMETERS

Parameter	Value
Input voltage, V_{in}	250 V
Output voltage, V_{out}	50 V
Maximum Current, I_{max}	4.25 A
Leakage inductance, L_{lk}	55 μH
Switching frequency, f_{sw}	100 kHz
Transformer turn ratio, n:1	3 : 1

The cubic equation, i.e., third-order polynomial equation, can be solved using either analytical or numerical approaches. In this paper, the analytic method known as the Cardano's formula is applied to solve the cubic equation, which could be digitally implemented in a microcontroller (MCU). The desired solution, i.e., the real root of the cubic equation, is obtained as (15). After $D_{\phi,ref}$ is derived, D_{ref} could be obtained from the quadratic equation in (13) as (16).

$$D_{\phi,ref} = sign(G_{V,ref})\cdot(-\frac{1}{3}) \\ [\alpha + \sqrt[3]{\alpha(\beta + \sqrt{\beta^2 - \alpha^4}} + \sqrt[3]{\alpha(\beta - \sqrt{\beta^2 - \alpha^4}}], \tag{15}$$

where $\beta = \alpha^2 - 13.5\left|G_{V,ref}\right|$.

$$D_{ref} = \frac{1-\sqrt{1-4\gamma}}{2}, \text{where } \gamma = \frac{1}{2\alpha}D_{\phi,ref}{}^2 + \left|D_{\phi,ref}\right|. \tag{16}$$

The flowchart of the 2-DOF modulation calculation is briefly described in Fig. 3. After the current reference, I_{ref}, is tracked by the voltage controller, the minimum current operation could be achieved by the model-based equations to calculate $D_{\phi,ref}$ and D_{ref}. $D_{\phi,ref}$ is changed within the range of [−0.25, 0.25] and D_{ref} is within the range of [0, 0.5] to transfer the maximum power in both directions.

Fig. 4 shows the trajectories of ($D_{\phi,ref}$, D_{ref}) according to I_{ref} variations where the proposed 2-DOF modulation is implemented. The system parameters are listed in Table I, where M is set to 0.6. For the light-load condition, $D_{\phi,ref}$ and D_{ref} are changed by the 2-DOF control where $D_{\phi,ref}$ and D_{ref} monotonically increases with the current references, I_{ref}. For the heavy-load condition, $D_{\phi,ref}$ increases gradually while D_{ref} is stuck on 0.5 where the 1-DOF control is applied. It shows the monotonic relationship between I_{ref} and $D_{\phi,ref}$ under $I_{ref} < |I_{max}|$, which means the 2-DOF

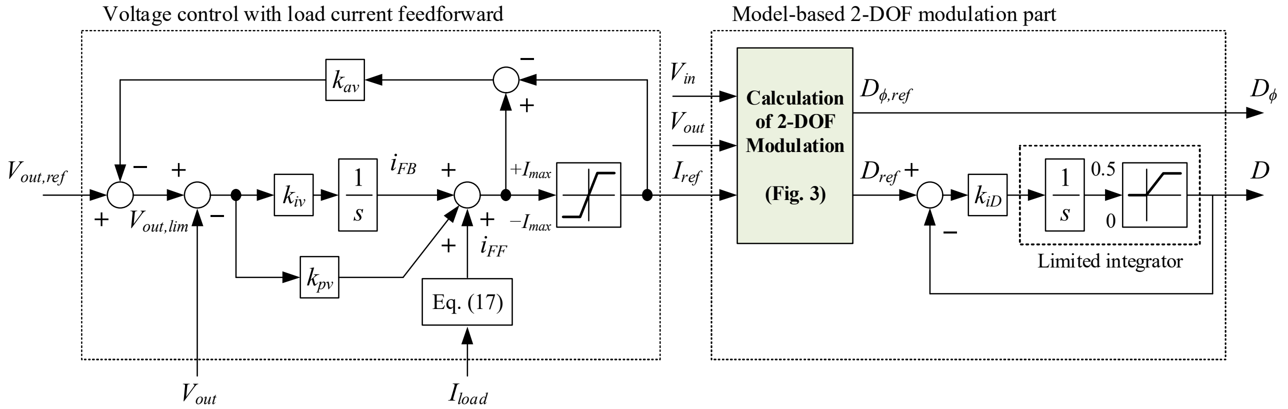

Fig. 5. Block diagram of the proposed unified voltage controller.

modulation control can be feasible as the closed-loop structure. However, the dynamics of ($D_{\phi,ref}$/ I_{ref}) and (D_{ref}/ I_{ref}) are highly nonlinear and changed depending on the operating condition. Therefore, the conventional PI controller without look-up tables (LUTs) is difficult to increase the dynamics.

IV. Proposed Unified Voltage Control Scheme

Fig. 5 shows the block diagram of the proposed unified controller. It consists of an error compensation part to minimize the effect of parameter errors and a model-based calculation part to improve the dynamics. The current reference, I_{ref}, is adjusted by the voltage controller with the load current feedforward and the anti-windup scheme. First, the PI control outputs the feedback current, i_{FB}, to compensate the voltage error, where the proportional gain, k_{pv}, responds directly to the output error, and the integral gain, k_{iv}, brings the error to zero.

Moreover, the feedforward path for the load current, I_{load}, is incorporated to decouple the effects of the load current disturbance. The feedforward current, i_{FF}, is modified to suppress positive feedback impacts caused by the load current path where the load is assumed to have resistive characteristics [9]. However, the positive feedback impacts are reversed in case of the regenerative operation, i.e., negative load current. Therefore, i_{FF} is multiplied with the voltage ratio between voltage reference and voltage output or vice versa as follows.

$$i_{FF} = \begin{cases} (V_{out,ref} / V_{out}) \cdot I_{load} & (I_{load} \geq 0) \\ (V_{out} / V_{out.ref}) \cdot I_{load} & (I_{load} \leq 0) \end{cases}. \tag{17}$$

Finally, an output limiter restricts the current reference under the current limit, I_{max}. I_{max} could be changed by thermal conditions of the DAHB system such as a maximum current limit of the half-bridge switches and/or an external temperature. The anti-windup scheme is applied to limit the output voltage reference within the realizable ranges, which could be adjusted by the anti-windup gain, k_{av}.

The modulation references, $D_{\phi,ref}$ and D_{ref}, are calculated based on the analytic equations in Fig. 3 as aforementioned. The transition between the 1-DOF and 2-DOF modulation is based on the calculated conductance criterion, $G_{v,cr}$. The modulation references trace the desired solution in a short time by applying the current reference, the input voltage, and the output voltage directly owing to the model-based structure. Thus, the proposed voltage controller unified with the 2-DOF modulation enhances the control dynamics under the input voltage and load current changes.

In this part, the duty reference determines the voltage ratio between upper and lower split capacitors. The abrupt changes of the duty reference provoke LC resonance where the split capacitor voltage is oscillated. Thus, the duty reference change is slow down by the integral controller and limited within [0, 0.5]. The transfer functions of the duty reference controller can be defined as follows.

$$\frac{D(s)}{D_{ref}(s)} = \frac{k_{iD}}{s + k_{iD}}, \tag{18}$$

where the dynamics are determined by the integral gain, k_{iD}.

V. Simulation Results

The simulation is carried out to evaluate the proposed voltage controller. The DAHB converter system is simulated in MATLAB/Simulink with PLECS where the parameters are set as Table I. The transformer includes a series resistance as a part of loss modeling within the converter.

Fig. 6 shows the output voltage and modulation reference waveforms under the load step changes from −4 A to +4 A in steps of 1.6 A increment every 50 ms, i.e., 37 % of the maximum current. The load is modeled as a current source to simulate the bi-directional power flow. It shows that the output voltage fluctuations are rapidly diminished in 20 ms due to the load current feedforward path. Moreover, $D_{\phi,ref}$ and D_{ref} are quickly changed to achieve the minimum rms current operation owing to the model-based calculation part. The voltage error induced by the converter loss is compensated by the proposed closed-loop PI controller.

Fig. 7 shows the transient responses when the output voltage reference and the input voltage step up or down by 10 % of the rated voltage. The load resistance is set as 21 Ω which dissipates 120 W at the rated voltage. It shows that the output voltage reference is quickly tracked by the proposed volage controller unified with the 2-DOF modulation. Moreover, the input voltage variation has a direct impact on the calculation part and the output voltage

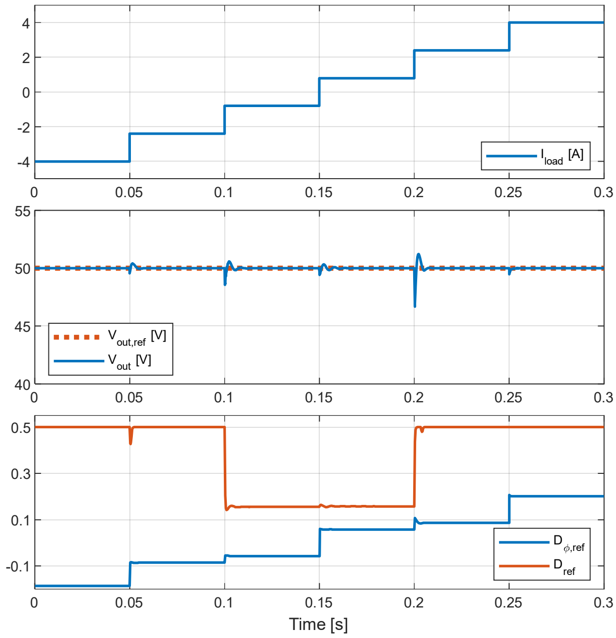

Fig. 6. Simulation results under load step changes.

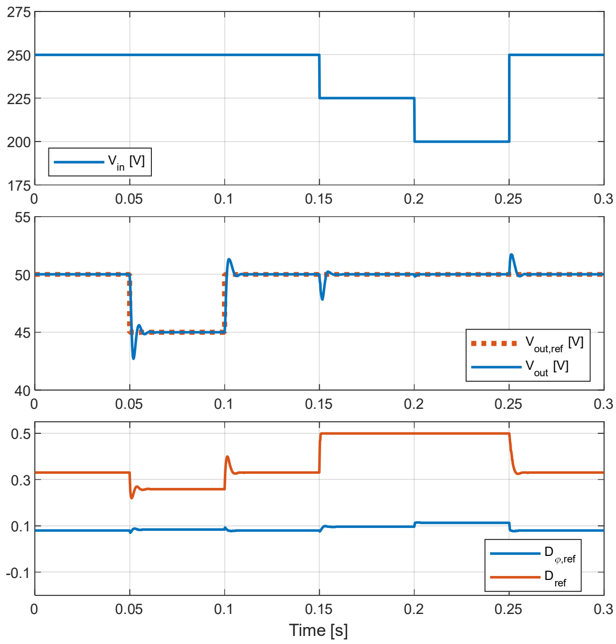

Fig. 7. Simulation results under input voltage fluctuations and output voltage reference changes.

reference affects the feedforward gain, which improves the dynamic performances while achieving the 2-DOF modulation.

VI. Experimental Results

The performance of the proposed voltage controller was also verified in a practical test setup, where the system parameters were identical to those in the simulation. The leakage inductance, L_{lk}, is the sum of an external inductance in series with the transformer and an inherent leakage inductance of the transformer. The algorithms were digitally implemented on a digital signal processor (DSP), TMS320F280049.

Fig. 8(a) shows the output voltage and modulation

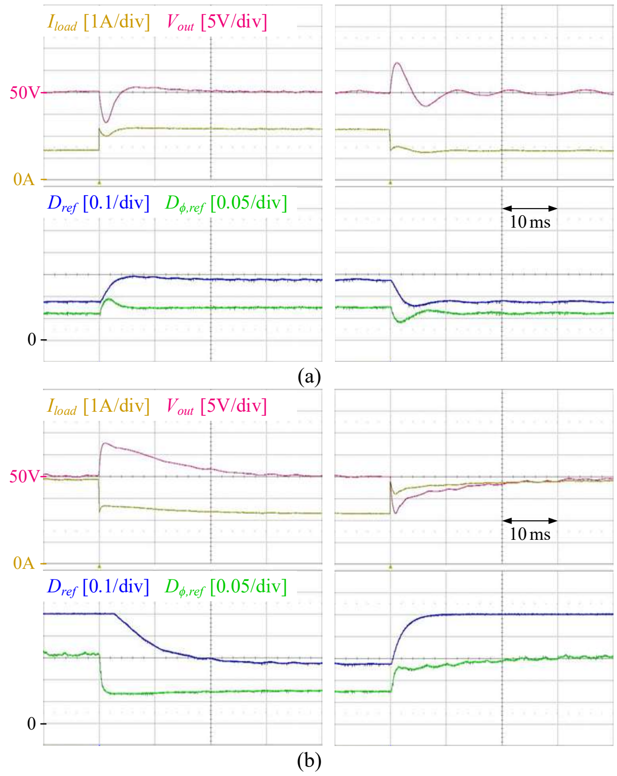

Fig. 8. Experimental results under load resistance variations between (a) 32 Ω and 21 Ω, (b) 21 Ω and 13 Ω.

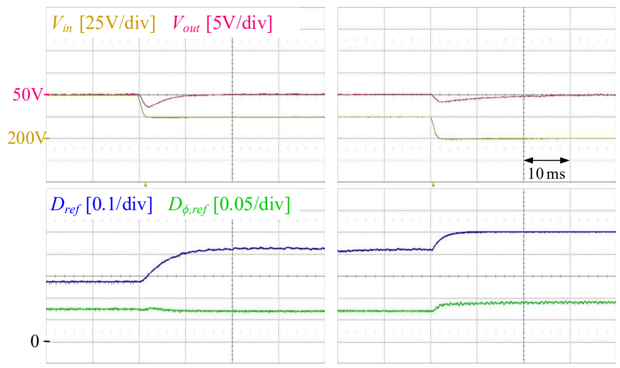

Fig. 9. Experimental results under input voltage changes.

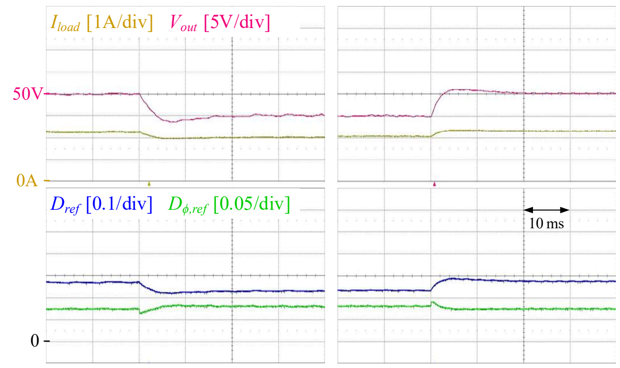

Fig. 10. Experimental results under output voltage reference changes.

reference waveforms when the load resistor is switched between 32 Ω and 21 Ω. The 2-DOF modulation scheme was applied to minimize rms current at both 37% load and 56% load, i.e., light-load conditions, where $D_{\phi,ref}$ and D_{ref} respond rapidly to the load current changes. Fig. 8(b) shows the waveforms under the load resistance variations between 21 Ω and 13 Ω. In this case, the 2-DOF modulation is changed to the 1-DOF modulation, where D_{ref} is quickly arrived at 0.5 under 90 % load, i.e., the heavy-load condition. The model-based calculation with the load current feedforward responds directly to the load resistance changes in 40 ms.

Fig. 9 shows the experimental waveforms when the input voltage decreases in steps of 25 V from 250 V to 200 V, where the load resistance was set to 21 Ω. The input voltage changes take effect immediately to the calculation part, where $D_{\phi,ref}$ and D_{ref} are calculated on the basis of the input voltage. The output voltage converges to the output voltage reference within 20 ms.

Fig. 10 shows the transient responses when the output voltage reference is changed from 50 V to 45 V and vice versa. Likewise, the load resistance was set to 21 Ω. The proposed voltage controller quickly responds to the output voltage reference changes under the 2-DOF modulation. The output voltage reference is tracked within 20 ms, where the output voltage error is minimized by the proposed closed-loop structure.

VII. Conclusions

This paper analyzes the minimum current operation of the DAHB converter where the phase shift and the duty ratio are control variables. Based on this analysis, the 2-DOF modulation scheme for the DAHB converter has been proposed for the bi-directional power flow. The model-based calculation part has been inserted to determine the phase shift reference and duty ratio reference where the virtual conductance is adopted to determine either 1-DOF or 2-DOF modulation. Moreover, the voltage controller with the load current feedforward has been applied to improve the dynamics while minimizing the error. The effectiveness of the proposed method is verified by the simulation and experimental results. The proposed method provides excellent dynamic performances even under the 2-DOF modulation scheme.

Acknowledgment

This research was supported by Technology Development Program to Solve Climate Changes through the National Research Foundation of Korea (NRF) funded by the Ministry of Science, ICT (2021M1A2A2065441).

References

[1] C. Mi, H. Bai, C. Wang, S. Gargies, "Operation, design and control of dual H-bridge-based isolated bidirectional DC–DC converter", *IET Power Electronics*, vol. 1, no. 4, pp. 507-517, Dec. 2008.

[2] N. Hou and Y. W. Li, "Overview and Comparison of Modulation and Control Strategies for a Nonresonant Single-Phase Dual-Active-Bridge DC–DC Converter," *IEEE Trans. Power Electron.*, vol. 35, no. 3, pp. 3148-3172, Mar. 2020.

[3] S. Shao, H. Chen, X. Wu, J. Zhang and K. Sheng, "Circulating Current and ZVS-on of a Dual Active Bridge DC-DC Converter: A Review," *IEEE Access*, vol. 7, pp. 50561-50572, 2019.

[4] J. Kim, H. -S. Song and K. Nam, "Asymmetric Duty Control of a Dual-Half-Bridge DC/DC Converter for Single-Phase Distributed Generators," *IEEE Trans. Power Electron.*, vol. 26, no. 3, pp. 973-982, Mar. 2011.

[5] M. S. Irfan, A. Ahmed, J. -H. Park and C. Seo, "Current-Sensorless Power-Decoupling Phase-Shift Dual-Half-Bridge Converter for DC–AC Power Conversion Systems Without Electrolytic Capacitor," *IEEE Trans. Power Electron.*, vol. 32, no. 5, pp. 3610-3622, May 2017.

[6] S. Chakraborty and S. Chattopadhyay, "Minimum-RMS-Current Operation of Asymmetric Dual Active Half-Bridge Converters With and Without ZVS," *IEEE Trans. Power Electron.*, vol. 32, no. 7, pp. 5132-5145, Jul. 2017.

[7] A. K. Jain and R. Ayyanar, "Pwm control of dual active bridge: Comprehensive analysis and experimental verification," *IEEE Trans. Power Electron.*, vol. 26, no. 4, pp. 1215-1227, Apr. 2011.

[8] W. Song, N. Hou and M. Wu, "Virtual Direct Power Control Scheme of Dual Active Bridge DC–DC Converters for Fast Dynamic Response," *IEEE Trans. Power Electron.*, vol. 33, no. 2, pp. 1750-1759, Feb. 2018.

[9] N. Hou, L. Ding, P. Gunawardena, Y. Zhang and Y. W. Li, "A Comprehensive Comparison of Two Fast-Dynamic Control Structures for the DAB DC– DC Converter," *IEEE Trans. Power Electron.*, vol. 37, no. 6, pp. 6488-6500, Jun. 2022.

[10] N. Hou, W. Song, Y. Li, Y. Zhu and Y. Zhu, "A Comprehensive Optimization Control of Dual-Active-Bridge DC–DC Converters Based on Unified Phase-Shift and Power-Balancing Scheme," *IEEE Trans. Power Electron.*, vol. 34, no. 1, pp. 826-839, Jan. 2019.